Autoinhibition regulates the motility of the *C. elegans* intraflagellar transport motor OSM-3

Miki Imanishi,[1,2,3] Nicholas F. Endres,[1,2] Arne Gennerich,[1,2] and Ronald D. Vale[1,2]

[1]Howard Hughes Medical Institute and [2]Department of Cellular and Molecular Pharmacology, University of California, San Francisco, San Francisco, CA 94107
[3]Institute for Chemical Research, Kyoto University, Uji, Kyoto 611-0011, Japan

OSM-3 is a Kinesin-2 family member from *Caenorhabditis elegans* that is involved in intraflagellar transport (IFT), a process essential for the construction and maintenance of sensory cilia. In this study, using a single-molecule fluorescence assay, we show that bacterially expressed OSM-3 in solution does not move processively (multiple steps along a microtubule without dissociation) and displays low microtubule-stimulated adenosine triphosphatase (ATPase) activity. However, a point mutation (G444E) in a predicted hinge region of OSM-3's coiled-coil stalk as well as a deletion of that hinge activate ATPase activity and induce robust processive movement. These hinge mutations also cause a conformational change in OSM-3, causing it to adopt a more extended conformation. The motility of wild-type OSM-3 also can be activated by attaching the motor to beads in an optical trap, a situation that may mimic attachment to IFT cargo. Our results suggest that OSM-3 motility is repressed by an intramolecular interaction that involves folding about a central hinge and that IFT cargo binding relieves this autoinhibition in vivo. Interestingly, the G444E allele in *C. elegans* produces similar ciliary defects to an *osm-3*–null mutation, suggesting that autoinhibition is important for OSM-3's biological function.

Introduction

Intraflagellar transport (IFT) of particles containing structural and signaling proteins is critical to building and maintaining cilia and flagella (Kozminski et al., 1993; Rosenbaum and Witman, 2002; Scholey, 2003). Defects in IFT in humans can give rise to dysfunctional cilia and produce a variety of disease states (Pazour and Rosenbaum, 2002). Sensory cilia in *Caenorhabditis elegans* neurons, which are crucial for chemosensory function (Perkins et al., 1986), also rely on IFT for their formation and function (Cole et al., 1998). Anterograde IFT transport in *C. elegans* sensory neurons is driven by two Kinesin-2 family members: heterotrimeric Kinesin-II and homodimeric OSM-3 (Cole et al., 1998; Signor et al., 1999b; Ou et al., 2005). Retrograde IFT transport is driven by a special class of dynein molecules that recycle the anterograde motor and proteins destined for turnover back to the cell body (Pazour et al., 1999; Signor et al., 1999a).

The activities of the heterotrimeric and homodimeric Kinesin-2 motor appear to be carefully regulated during IFT. Microscopy studies in living *C. elegans* have shown that both motors cooperate to move IFT particles along the middle segment of the cilia consisting of nine doublet microtubules, whereas only OSM-3 transports IFT particles along the distal segment consisting of nine singlet microtubules (Snow et al., 2004; Evans et al., 2006). OSM-3 activity is most likely confined to axonemes in *C. elegans* because *osm-3*–null animals only display a loss of the distal segments of their sensory cilia. Thus, it is possible that the OSM-3 motor is active only in the cilium, where it executes its transport functions. However, the mammalian homologue of Osm-3 (KIF17) is involved in both ciliary IFT (Setou et al., 2000) and membrane transport in neuron dendrites (Setou et al., 2000).

To better understand the molecular basis of IFT transport, it is important to characterize the properties of the IFT motor proteins in vitro. Although several studies have explored the motile properties of the heterotrimeric Kinesin-2 motor in vitro (Cole et al., 1993; Yamazaki et al., 1995; Zhang and Hancock, 2004), in vitro studies of OSM-3 and single-molecule studies of KIF17 have not been undertaken. In this study, using single-molecule techniques, we show that single OSM-3 molecules do not move processively (long distance movement along microtubules without dissociation) in vitro. However, motility can be activated by attaching OSM-3 via its tail domain to beads or by mutations to a hinge region in the middle of the molecule. These results support a model in which OSM-3 is autoinhibited in a folded conformation and processive movement is activated by attachment to IFT cargo. This mechanism is similar to an

M. Imanishi and N.F. Endres contributed equally to this paper.

Correspondence to Ronald D. Vale: vale@cmp.ucsf.edu

Abbreviations used in this paper: IFT, intraflagellar transport; TIRF, total internal reflection fluorescence.

The online version of this article contains supplemental material.

The Journal of Cell Biology, Vol. 174, No. 7, September 25, 2006 931–937
http://www.jcb.org/cgi/doi/10.1083/jcb.200605179

intramolecular, autoinhibitory interaction in Kinesin-1 that has been proposed to keep this motor in an inactive conformation until it interacts with its cargo (for review see Adio et al., 2006). The biological importance of OSM-3 autoinhibition is suggested by the finding that constitutive activation of OSM-3 motility through a single point mutation also causes severe defects in IFT transport.

Results and discussion

Here, we have characterized the motile properties of a recombinant OSM-3 construct consisting of full-length OSM-3 (aa 1–699) with a C-terminal GFP (Fig. 1). As expected, OSM-3 was an active plus end–directed motor in a microtubule gliding assay, although the velocity of movement (0.3 μm/s) in this gliding assay was lower than IFT transport by OSM-3 in the distal segment (1.3 μm/s; Snow et al., 2004). The ATP hydrolysis k_{cat} of the full-length OSM-3 motor was only 4 ATP/s/head (Table I and Fig. S1, available at http://www.jcb.org/cgi/content/full/jcb.200605179/DC1), which is much slower than would be expected for a motor capable of moving 300–1,300 nm/s (assuming that it takes 8-nm steps per ATP hydrolyzed as shown for Kinesin-1; Svoboda et al., 1993). We next examined OSM-3 processivity by imaging single GFP-labeled molecules using a total internal reflection fluorescence (TIRF) microscope. In this assay, a truncated construct of Kinesin-1 (K530; Table I) fused to GFP exhibited numerous processive movements with a mean run length of 1.2 μm, which is similar to previous results (Romberg et al., 1998). In contrast, full-length OSM-3 rarely showed any processive runs (Video 1).

OSM-3's lack of processivity is somewhat surprising because many dimeric motors involved in long-range transport are processive in vitro (Howard et al., 1989; Mehta et al., 1999; Tomishige et al., 2002; Zhang and Hancock, 2004). Extensive in vitro studies on the long-range, unidirectional processivity of Kinesin-1 and -3 have identified three critical determinants of processivity: (1) the presence of a stable neck coiled coil that joins the two kinesin motor domains immediately after the neck linker (kinesin's mechanical element) (Romberg et al., 1998; Al-Bassam et al., 2003; Bathe et al., 2005); (2) the ability of the two motor domains to coordinate their ATPase cycles (Hackney, 1994; Ma and Taylor, 1997; Gilbert et al., 1998); and (3) the presence of intramolecular interactions that inhibit processivity (Hackney et al., 1992; Coy et al., 1999; Friedman and Vale, 1999; Al-Bassam et al., 2003). We sought to test whether any of these possible mechanisms could explain the lack of processivity by OSM-3.

We initially suspected that an unstable neck may underlie the lack of OSM-3 processivity because the neck coiled coil of OSM-3 is more than two heptads shorter and is predicted to be much weaker than the neck coiled coil of Kinesin-1 (Fig. 1 b). The putative OSM-3 neck coiled coil is also less positively charged than the neck coiled coil of Kinesin-1, a factor shown to enhance its processivity (Thorn et al., 2000). We tested the hypothesis that a weak coiled coil may be responsible for the lack of processivity of OSM-3 by fusing the putative neck coiled coil of OSM-3 (and the subsequent C-terminal stalk and tail domains) to the motor domain and neck linker of Kinesin-1

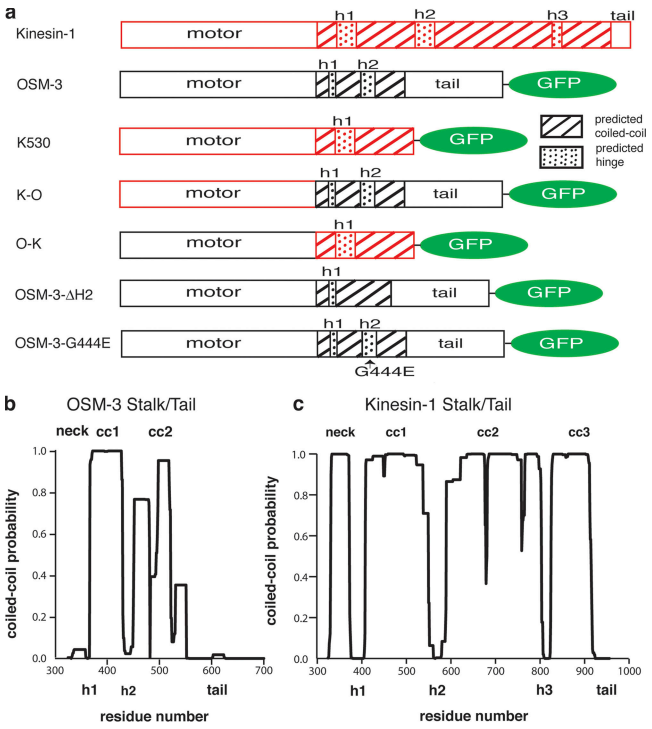

Figure 1. **Domain architecture of OSM-3, Kinesin-1, and OSM-3 constructs used in this study.** (a) Domain architecture reveals the positions of the motor and tail domains as well as predicted coiled coils and hinges (see panel b). Domain sizes are shown roughly proportional to the length of the sequence in each domain. Kinesin-1 and OSM-3 sequences are colored red and black, respectively. (b) Coiled-coil prediction (based upon COILS; Lupas et al., 1991) for Kinesin-1 (residues 337–950) and OSM-3 (residues 338–699). Neck, hinge, and coiled-coil subdomains are labeled.

(K-O; Table I). We reasoned that if the OSM-3 neck was incompatible with processivity, K-O should be a nonprocessive motor. Contrary to this prediction, K-O molecules moved processively in the single molecule TIRF assay with similar velocities (0.5 ± 0.2 μm/s), albeit with reduced run lengths (0.4 μm), compared with K530 (0.7 ± 0.3 μm/s and 1.2 μm). The processivity of K-O suggests that the OSM-3 neck coiled coil is not responsible for the lack of processivity in OSM-3.

We next tested whether the OSM-3 motor domain was incompatible with efficient processive motility by fusing the OSM-3 motor domain (catalytic core and neck linker) to the neck coiled coil and stalk of Kinesin-1 (O-K; Table I). O-K exhibited robust processive movement with a mean run length (2.6 μm) that was approximately twofold higher than that of K530. The velocity measured in the single-molecule fluorescent assay (1.5 ± 0.3 μm/s) was similar to the velocity of OSM-3 cargo in vivo (1.3 ± 0.2 μm/s), suggesting that O-K may be mimicking the in vivo function of the motor. Thus, the OSM-3 motor domain is compatible with processivity in a dimeric construct that lacks its native stalk/tail domain. Interestingly, the O-K ATPase rate ($k_{cat,}$ 75 ATP/s/head; Table I and Fig. S1) was an order of magnitude greater than that of wild-type OSM-3 ($k_{cat,}$ 4 ATP/s/head). This difference in rates indicates that some element C terminal to the motor domain of OSM-3 is inhibiting its catalytic activity and likely the processivity of the motor as well.

Table I. **Motility and ATPase properties of constructs used in this study**

Constructs	Single molecule		Gliding	ATPase activity	
	Velocity	Run length	Velocity	k_{cat}	K_m MT
	μm/s	*μm*	*μm/s*	*ATPs/s/head*	*μM*
Osm-3	RD	RD	0.32 ± 0.06	4 ± 1	0.23 ± 0.02
K530	0.7 ± 0.3	1.2	ND	29 ± 6	0.29 ± 0.08
K-O	0.5 ± 0.2	0.4	0.30 ± 0.07	33 ± 5	0.20 ± 0.10
O-K	1.5 ± 0.3	2.6	0.48 ± 0.08	75 ± 9	0.13 ± 0.09
OSM-3–ΔH2	0.8 ± 0.2	1.9	0.80 ± 0.10	69 ± 5	0.21 ± 0.06
OSM-3–G444E	1.1 ± 0.2	1.4	0.91 ± 0.09	75 ± 2	0.30 ± 0.10

Motor protein constructs were purified, and assays were conducted as described in Materials and methods. For motility data, >100 measurements were taken from at least two protein preparations. Velocities shown represent the mean and SD. Run lengths were corrected for photobleaching (Thorn et al., 2000), and the indicated mean run lengths were determined by fitting run length histograms to an exponential decay function. The mean and SD of the ATPase data were derived from three to nine assays (as shown in Fig. S1, available at http://www.jcb.org/cgi/content/full/jcb.200605179/DC1) using two to four protein preparations. RD, rarely detected; Osm-3 did not exhibit consistent processive motion (only a few short runs detected in >30 min of observation; consistent for five protein preparations). MT, microtubule.

To test whether the tail domain might inhibit the processivity of OSM-3, we made a construct of OSM-3 lacking the tail domain (OSM-3 aa 1–555) but found that it was an unstable dimer under conditions of the TIRF assay (low nanomolar range; unpublished data). An alternative strategy for investigating a possible autoinhibition of OSM-3 processivity was suggested by a comparison with Kinesin-1. The processivity of Kinesin-1 is inhibited by an autoinhibitory interaction between its neck coiled coil and tail domains (Hackney and Stock, 2000; for review see Adio et al., 2006). The interaction of these distant N- and C-terminal elements is achieved by folding about a flexible hinge in the stalk (Fig. 1 b, H2). The deletion of this hinge prevents autoinhibition and restores processivity to the motor (Friedman and Vale, 1999). A comparison of the overall architecture of the Kinesin-1 and OSM-3 stalk suggested the presence of an analogous hinge in OSM-3 (Fig. 1 b, H2). Therefore, we wondered whether the deletion of H2 and the in-phase fusion of the adjacent coiled coils (Fig. 1 b, cc1 and cc2) could restore processivity to OSM-3. Strikingly, this construct (OSM-3–ΔH2) exhibited robust processive movement with long run lengths (~2 μm; Table I and Video 2, available at http://www.jcb.org/cgi/content/full/jcb.200605179/DC1) in the single-molecule TIRF assay and displayed similar elevated ATPase rates (~70 ATP/s/head) to O-K. The dramatic activation of processivity in OSM-3–ΔH2 demonstrates that the OSM-3 motor, in the absence of any fusion to Kinesin-1, has an intrinsic potential for processive motion. These results also show that H2 plays a critical role in repressing the processivity and microtubule-stimulated ATPase activity of OSM-3.

Having demonstrated the importance of H2 for the regulation processivity in vitro, we searched through OSM-3 alleles for mutations in H2 that produce chemosensory defects in *C. elegans* (Snow et al., 2004). We noticed one allele (*sa125*) in H2 that changed a glycine to a glutamatic acid (G444E). When this H2 point mutation was introduced into full-length OSM-3 (OSM-3–G444E), we found a striking activation of processivity and ATPase activity (75 ATP/s/head) similar to that observed with the deletion of the entire H2 region. The velocity of OSM-3–G444E (1.1 ± 0.2 μm/s) is also similar to that of OSM-3–driven IFT transport in vivo, implying that this mutation could activate OSM-3 in a manner similar to its activation in vivo. This dramatic activation of motility by a single point mutant implies that a specific conformation of H2 is required for the regulation of OSM-3 motility.

In Kinesin-1, H2 facilitates a conformational transition between a compact, nonprocessive form (S = 6.7) and a more extended processive form (S = 5.1; Hackney et al., 1992) . The compact to extended conformational transition is favored by cargo binding (Coy et al., 1999) and high ionic strength (Hackney et al., 1992). To investigate whether a similar conformational change could underlie the regulation of OSM-3 processivity, we examined the hydrodynamic properties of wild-type and mutant OSM-3 by sucrose gradient sedimentation (Fig. 2). Similar to Kinesin-1, OSM-3 sediments with a higher $S_{20,w}$ value at low ionic strength ($S_{20,w}$ = 7.9) than at high ionic strength ($S_{20,w}$ = 6.8), suggesting that it too has compact and extended conformations. In contrast to wild-type OSM-3, the H2 mutants (OSM-3–ΔH2 and OSM-3–G444E) sedimented with a low $S_{20,w}$ value ($S_{20,w}$ = 6.5–6.9) at both low and high ionic strengths. These results suggest that the processive H2 mutants stabilize an extended conformation of OSM-3. We attempted to visualize the two OSM-3 conformations by rotary shadow EM but unfortunately could not obtain satisfactory images as a result of aggregation of the motor on the mica surface (unpublished data). The correlation between the extended conformation of OSM-3 and in vitro processivity suggests that a reversible autoinhibitory interaction regulates the motility of OSM-3.

Relief of OSM-3 autoinhibition in vivo might be stimulated by cargo binding. To mimic cargo binding in vitro, we attached wild-type OSM-3 and OSM-3–G444E via their C- terminal GFP to beads coated with GFP antibody. Motor- coated beads were then captured by an optical trap and positioned near axonemes immobilized onto a coverslip. As expected, OSM-3–G444E-coated beads moved processively at three different constant loads generated by force feedback (1–6 pN; Fig. 3 a). In a stationary (nonfeedback) optical trap, the motor dissociated before reaching a stall force (cessation of forward motion when the opposing force of the optical trap equals the maximum force produced by the motor). However, the observation of movement

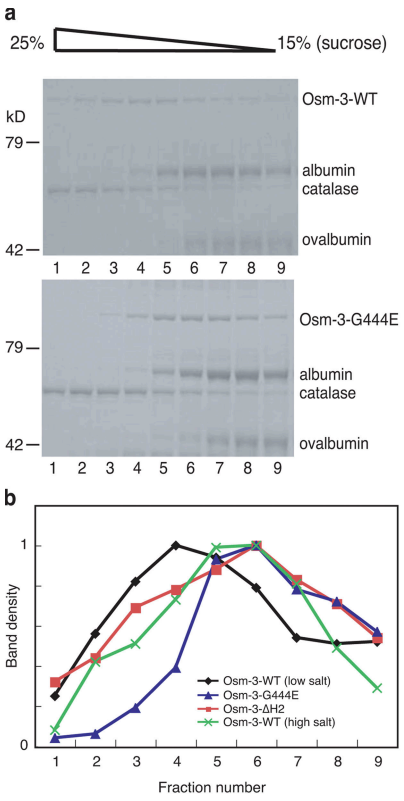

c

Constructs	Sucrose Gradient $S_{20,w}$	
	Low salt	High salt
Osm-3-WT	7.9 ± 0.6	6.8 ± 0.2
Osm-3-G444E	6.8 ± 0.4	6.5
Osm-3-ΔH2	6.9 ± 0.4	6.7

Figure 2. **Hydrodynamic properties of wild-type OSM-3 and H2 mutants measured by sucrose gradient sedimentation.** (a) Fractions from sucrose gradients (0 M NaCl) analyzed by SDS-PAGE. Note the shift in the sedimentation peak of OSM-3–G444E compared with wild-type OSM-3. Albumin, catalase, and ovalbumin were added as hydrodynamic standards. (b) Normalized SDS-PAGE band intensities are plotted versus fraction number for OSM-3, OSM-3–ΔH2, and OSM-3–G444E at 0 M NaCl and for wild-type (WT) OSM-3 at 1 M NaCl. (c) Table summarizing the $S_{20,w}$ values measured for the three constructs at low (0 and 0.05 M) or high (0.5 and 1 M) NaCl. Values represent the mean ± SD for six to seven independent experiments for low salt. The high-salt values are from four experiments with wild type and from a single experiment with the mutants. Values from individual sucrose gradients are reported in Table S1 (available at http://www.jcb.org/cgi/content/full/jcb.200605179/DC1).

with a force feedback trap at 6 pN indicates that the motor can exert forces in excess of that value and, thus, appears to have similar force-producing capability to Kinesin-1 (Svoboda and Block, 1994). Wild-type OSM-3–coated beads also moved processively with velocities comparable with OSM-3–G444E at all three force levels (Fig. 3 b), implying a similar mechanism.

To determine whether the bead motion was driven by single or multiple motors, the fraction of moving beads was measured as a function of the motor/bead ratio. Poisson statistical analysis clearly revealed that a single OSM-3–G444E or wild-type OSM-3 motor is sufficient to move a bead (Fig. 3, c and d; Svoboda and Block, 1994), although wild-type OSM-3 required a 60-fold higher motor/bead ratio to yield an equivalent probability of bead movement as OSM-3–G444E. The requirement for a higher concentration of wild-type OSM-3 could be caused by a lower probability of motor-bead attachment as a result of the folded conformation of the inactivated OSM-3 or as a result of inefficient activation of the repressed OSM-3 motors by their attachment to the GFP antibody-coated beads. The fact that wild-type OSM-3 bound to anti-GFP antibody-coated glass slides can move microtubules in a gliding assay also is consistent with the idea that surface attachment can activate repressed OSM-3, although the number of active motors was not investigated in this assay. In summary, our results demonstrate that wild-type OSM-3, once relieved of its inhibition by surface attachment, is capable of processive movement.

In conclusion, we have shown that the processive movement and microtubule-stimulated ATPase activity of OSM-3 are repressed in solution. ATPase activity and processivity are both dramatically stimulated by mutations in hinge 2, which also change the conformation of the motor from a compact to an extended form. Wild-type OSM-3 also becomes processive when attached via its tail domain to beads. Collectively, these results suggest a model in which OSM-3 exists in the cytoplasm in a compact, autoinhibited state and that binding to an IFT particle relieves this autoinhibition, converting the motor to an extended conformation and enabling long-distance processive movement (Fig. 4).

Although more work will be needed to understand the structural basis of this autoinhibition, the processivity of OSM-3–Kinesin-1 chimeras (O-K and K-O) suggests that inhibition requires both the OSM-3 motor and stalk/tail domains and perhaps involves interactions between the two. This proposed regulatory mechanism for OSM-3 is similar to that described for Kinesin-1 (for review see Adio et al., 2006). However, these two motors belong to different kinesin classes that share no sequence similarity in their nonmotor domains, having diverged very early in eukaryotic evolution (Vale, 2003), and, thus, the structural details of autoinhibition are likely to differ. Kinesin-3 processivity also is repressed by the formation of an intramolecular coiled coil in its neck region, which inhibits dimerization (Al-Bassam et al., 2003). Although the effects on motor activity are not known, heterotrimeric Kinesin-II also undergoes a salt-dependent conformational shift between a compact and an extended form (Wedaman et al., 1996). Thus, autoinhibitory mechanisms, although differing in their precise intramolecular interactions, may be commonly used in motor regulation. It will be interesting to explore whether KIF17, the mammalian homologue of OSM-3 involved in olfactory cilia IFT and neuronal transport in dendrites (Setou et al., 2000; Jenkins et al., 2006), is also regulated by an autoinhibitory mechanism similar to OSM-3.

The regulation of OSM-3 processivity is likely to be important for its biological function in vivo. Strongly supporting this connection, the OSM-3–G444E allele (*sa125*), which interferes with autoinhibition in vitro, behaves indistinguishably from the OSM-3–null allele (*sa131*) in *C. elegans* chemosensory neurons (Snow et al., 2004). Further supporting a loss of OSM-3 function, the distal ciliary segment (which is supplied

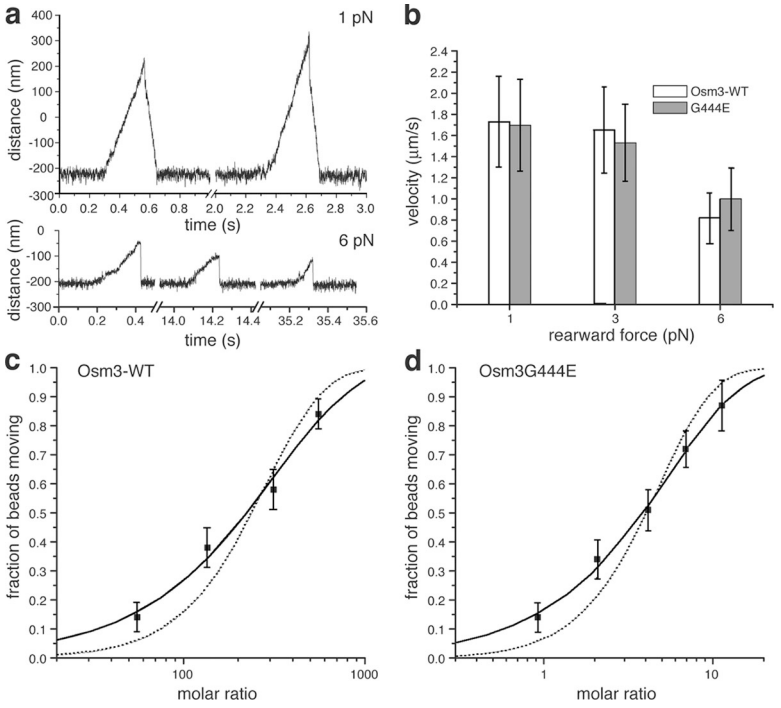

Figure 3. **Single wild-type OSM-3 and OSM-3–G444E are processive motors in an optical trapping bead assay.** (a) Processive movement of wild-type OSM3 under a constant rearward load of 1 pN (top; two consecutive runs from the same record are shown; k = 0.024 pN/nm) and 6 pN (bottom; three runs from the same record are depicted; k = 0.044 pN/nm). Bead movement was analyzed in a detection area of ±200 nm within which the motor experiences a constant load from the feedback-controlled optical trap. (b) Motor velocity as a function of rearward load for both wild-type (WT) OSM-3 and OSM-3–G444E. Values are shown as the mean ± SD (error bars). (c) The fraction of wild-type OSM-3–coated beads binding to and moving along axonemes as a function of the ratio of the motor/bead concentration. The bead concentration was kept constant for all measurements at 4 pM, whereas the motor concentration was varied. The solid line represents the fit to the Poisson distribution $1 - \exp(-\lambda C)$ for one or more motor molecules (reduced $x^2 = 0.31$; Svoboda and Block, 1994). The dotted line represents the fit to the distribution $1 - \exp(-\lambda C) - (\lambda C)\exp(-\lambda C)$ for two or more molecules (reduced $x^2 = 2.93$). Data values are displaced as the mean ± the square root of (f[1−f]/N), with N being the number of beads tested. (d) The fraction of beads moving as a function of the ratio of Osm-3–G444E and bead concentration. The solid line depicts the fit to the Poisson distribution for one or more motor molecules (reduced $x^2 = 0.08$), and the dotted line represents the fit to the distribution for two or more motor molecules (reduced $x^2 = 2.01$).

exclusively by OSM-3 transport; Snow et al., 2004) does not form in OSM-3–G444E mutant animals, and IFT particles move along the remaining ciliary segment at velocities similar to IFT particles being transported by heterotrimeric Kinesin-II alone (Ou, G., and J. Scholey, personal communication). Although the OSM-3–G444E allele (*sa125*) behaves as a null mutation in vivo, our in vitro optical trapping experiments show that its velocity and force production are indistinguishable from the wild-type motor. Thus, the most plausible explanation for the in vivo mutant phenotype is a loss of motor regulation rather than motor domain dysfunction.

Two possible mechanisms could explain how a loss of autoinhibition gives rise to a null phenotype. First, a constitutively active OSM-3–G444E motor may not be able to dock onto IFT cargo. Second, processive OSM-3–G444E motors may constitutively move along microtubules in the neuronal cell body and fail to be delivered to the cilium. Another open question is how OSM-3 is relieved of its autoinhibition. It has been shown previously that the DYF-1 protein is required to load OSM-3 onto IFT particles (Ou et al., 2005), but purified DYF-1 did not activate wild-type OSM-3 in our single-molecule assay (unpublished data). Thus, the regulatory machinery may require additional proteins or posttranslational modifications. Consistent with this idea, two novel mutants with a similar phenotype to *dyf-1* and *osm-3* worms were recently identified (Ou, G., and J. Scholey, personal communication). The ability to study OSM-3 autoinhibition in in vitro and in living *C. elegans* provides powerful tools for dissecting the regulatory mechanism of this IFT motor.

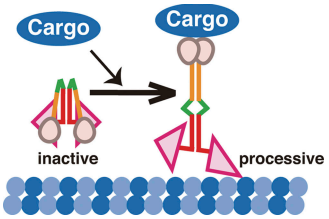

Figure 4. **Autoinhibitory model of OSM-3 motor regulation.** Cargo attachment converts the intramolecular folded, repressed OSM-3 motor into an extended conformation that can undergo processive motion. See Results and discussion for details.

Materials and methods

Cloning and protein preparations

OSM-3 cDNA was obtained from J. Scholey (University of California, Davis, Davis, CA). From this clone, we constructed OSM-3–GFP in a pET-17bplasmid, which encodes aa 1–699 of *C. elegans* OSM-3 with a C-terminal GFP (S65T variant) followed by a His_6 tag. K530-GFP (aa 1–530 of Kinesin-1) was derived from K560-GFP (Friedman and Vale, 1999). In the O-K construct, aa 1–337 of the OSM-3 motor domain were followed by aa 337–530 of the K530 stalk. In the K-O construct, aa 1–336 of the human Kinesin-1 motor domain were followed by aa 338–699 of the OSM-3 stalk/tail. The OSM-3–G444E construct was created by QuikChange mutagenesis (Stratagene). For OSM-3–ΔH2, aa 428–447 were removed to maintain a continuous heptad repeat between cc1 and cc2 (Fig. 1). Protein expression and purification were performed as described previously (Case et al., 1997). For ATPase assays, single-molecule fluorescence and optical trap experiments, and gliding assays, motor proteins were further purified by microtubule affinity (Case et al., 1997). Motor concentration was determined either by Bradford assay or SDS-PAGE using BSA as a standard.

ATPase assays and single-molecule fluorescence measurements

Microtubule-stimulated ATPase activities were measured as described previously (Woehlke et al., 1997) using 1–20 nM of motor and 0–10 μM of microtubules in BRB12 (12 mM Pipes, pH 6.8, 2 mM $MgCl_2$, 1 mM EGTA, 1 mM DTT, and 1 mM ATP). The hydrolysis of ATP was plotted against microtubule concentration, and data were fitted to a Michealis-Menton equation to determine the k_{cat} and K_m microtubule. The movements of single GFP-fused kinesin molecules along axonemes were visualized by TIRF microscopy using BRB25 buffer (BRB12 with 25 mM Pipes) as described previously (Pierce and Vale, 1998). The laser power for total internal reflection illumination was 9 mW. Motility was analyzed and corrected for photobleaching using

ImageJ software (National Institutes of Health) as described previously (Thorn et al., 2000). Microtubule gliding assays were performed using a glass slide coated with GFP antibodies, and gliding velocities of Cy3-labeled microtubules were determined as described previously (Case et al., 1997). We found that the microtubule gliding velocities of wild-type OSM-3 are closer to those of the OSM-3 hinge mutant when the wild-type motor is adsorbed directly to glass rather than via surface-coated GFP antibodies.

Hydrodynamic analysis

Sucrose density centrifugation was performed in BRB25 and 10 μM ATP with 0, 0.05, 0.5, or 1 M NaCl. OSM-3 and standard calibration proteins (ovalbumin, 3.7 S; albumin, 4.2 S; and catalase, 11.3 S) were mixed and loaded onto 12–33% sucrose gradients. After centrifugation at 50,000 *g* for 6 h using a SW55Ti rotor (Beckman Coulter), fractions were analyzed by SDS-PAGE. $S_{20,w}$ values of the standards were plotted versus their peak sedimentation fraction number and fit to a linear curve. $S_{20,w}$ of the OSM-3 motor were calculated based upon their peak sedimentation fraction and the slope of the standard curve.

Optical trapping assay

The optical trapping bead assay was performed using a feedback-controlled single-beam trapping microscope. GFP-tagged OSM-3 and OSM-3–G444E were coupled to carboxylated latex beads (0.92-μm diameter; Invitrogen) via affinity-purified anti-GFP antibodies (Tomishige et al., 2002). Trapped beads were positioned near rhodamine-labeled sea urchin sperm flagellar axonemes immobilized onto a coverslip. Bead displacement was sampled at 2 kHz with a quadrant photodiode detector. Trap stiffness was calibrated for each trapped bead from the amplitude of the thermal diffusion. Before each experiment, the trapped bead was scanned along the x axis (coinciding with the long axis of the axoneme) across the detection region to obtain the detector's response. Experiments were performed at dilutions at which the fraction of beads moving was ≤0.3 to ensure measurements on a single-molecule level (Svoboda et al., 1994). Velocities were obtained from the slopes of the displacement traces of the beads moving under constant load. The bead-trap separation during force-clamp measurements was between 50 and 150 nm, depending on applied load (1–6 pN) and trap stiffness (0.022–0.06 pN/nm). The assay solution consisted of 80 mM Pipes, pH 6.8, 2 mM $MgCl_2$, 1 mM EGTA, 1 mM Mg-ATP, 1 mg/ml casein, 10 mM DTT, and an oxygen scavenger system (Yildiz et al., 2003).

Online supplemental material

Video 1 shows that wild-type OSM-3–GFP does not move processively along axonemes. Videos 2 and 3 show the processive motion of OSM-3–ΔH2-GFP and OSM-3–G444E-GFP, respectively, along axonemes. Fig. S1 shows the microtubule-stimulated ATPase activity of wild-type OSM-3 and OSM-3 mutants and chimeras. Table S1 is a summary of individual sucrose gradient data for wild-type and OSM-3 hinge mutants. Online supplemental material is available at http://www.jcb.org/cgi/content/full/jcb.200605179/DC1.

We thank J. Scholey, G. Ou, and X. Pan for helpful discussions. We also thank J. Heuser for help with EM.

This work was supported by the National Institutes of Health (grant to R.D. Vale), Jane Coffins Child Foundation (grant to A. Gennerich), and the German Research Foundation (grant GE 1609/1 to A. Gennerich).

Submitted: 31 May 2006
Accepted: 22 August 2006

References

Adio, S., J. Reth, F. Bathe, and G. Woehlke. 2006. Review: regulation mechanisms of Kinesin-1. *J. Muscle Res. Cell Motil.* 27:153–160.

Al-Bassam, J., Y. Cui, D. Klopfenstein, B.O. Carragher, R.D. Vale, and R.A. Milligan. 2003. Distinct conformations of the kinesin Unc104 neck regulate a monomer to dimer motor transition. *J. Cell Biol.* 163:743–753.

Bathe, F., K. Hahlen, R. Dombi, L. Driller, M. Schliwa, and G. Woehlke. 2005. The complex interplay between the neck and hinge domains in kinesin-1 dimerization and motor activity. *Mol. Biol. Cell.* 16:3529–3537.

Case, R.B., D.W. Pierce, N. Hom-Booher, C.L. Hart, and R.D. Vale. 1997. The directional preference of kinesin motors is specified by an element outside of the motor catalytic domain. *Cell.* 90:959–966.

Cole, D.G., S.W. Chinn, K.P. Wedaman, K. Hall, T. Vuong, and J.M. Scholey. 1993. Novel heterotrimeric kinesin-related protein purified from sea urchin eggs. *Nature*. 366:268–270.

Cole, D.G., D.R. Diener, A.L. Himelblau, P.L. Beech, J.C. Fuster, and J.L. Rosenbaum. 1998. Chlamydomonas kinesin-II-dependent intraflagellar transport (IFT): IFT particles contain proteins required for ciliary assembly in *Caenorhabditis elegans* sensory neurons. *J. Cell Biol.* 141:993–1008.

Coy, D.L., W.O. Hancock, M. Wagenbach, and J. Howard. 1999. Kinesin's tail domain is an inhibitory regulator of the motor domain. *Nat. Cell Biol.* 1:288–292.

Evans, J.E., J.J. Snow, A.L. Gunnarson, G. Ou, H. Stahlberg, K.L. McDonald, and J.M. Scholey. 2006. Functional modulation of IFT kinesins extends the sensory repertoire of ciliated neurons in *Caenorhabditis elegans*. *J. Cell Biol.* 172:663–669.

Friedman, D.S., and R.D. Vale. 1999. Single-molecule analysis of kinesin motility reveals regulation by the cargo-binding tail domain. *Nat. Cell Biol.* 1:293–297.

Gilbert, S.P., M.L. Moyer, and K.A. Johnson. 1998. Alternating site mechanism of the kinesin ATPase. *Biochemistry*. 37:792–799.

Hackney, D.D. 1994. Evidence for alternating head catalysis by kinesin during microtubule-stimulated ATP hydrolysis. *Proc. Natl. Acad. Sci. USA*. 91:6865–6869.

Hackney, D.D., and M.F. Stock. 2000. Kinesin's IAK tail domain inhibits initial microtubule-stimulated ADP release. *Nat. Cell Biol.* 2:257–260.

Hackney, D.D., J.D. Levitt, and J. Suhan. 1992. Kinesin undergoes a 9 S to 6 S conformational transition. *J. Biol. Chem.* 267:8696–8701.

Howard, J., A.J. Hudspeth, and R.D. Vale. 1989. Movement of microtubules by single kinesin molecules. *Nature*. 342:154–158.

Jenkins, P.M., T.W. Hurd, L. Zhang, D.P. McEwen, R.L. Brown, B. Margolis, K.J. Verhey, and J.R. Martens. 2006. Ciliary targeting of olfactory CNG channels requires the CNGB1b subunit and the Kinesin-2 motor protein, KIF17. *Curr. Biol.* 16:1211–1216.

Kozminski, K.G., K.A. Johnson, P. Forscher, and J.L. Rosenbaum. 1993. A motility in the eukaryotic flagellum unrelated to flagellar beating. *Proc. Natl. Acad. Sci. USA*. 90:5519–5523.

Lupas, A., M. Van Dyke, and J. Stock. 1991. Predicting coiled coils from protein sequences. *Science*. 252:1162–1164.

Ma, Y.-Z., and E.W. Taylor. 1997. Interacting head mechanism of microtubule-kinesin ATPase. *J. Biol. Chem.* 272:724–730.

Mehta, A.D., R.S. Rock, M. Rief, J.A. Spudich, M.S. Mooseker, and R.E. Cheney. 1999. Myosin-V is a processive actin-based motor. *Nature*. 400:590–593.

Ou, G., O.E. Blacque, J.J. Snow, M.R. Leroux, and J.M. Scholey. 2005. Functional coordination of intraflagellar transport motors. *Nature*. 436:583–587.

Pazour, G.J., and J.L. Rosenbaum. 2002. Intraflagellar transport and cilia-dependent diseases. *Trends Cell Biol.* 12:551–555.

Pazour, G.J., B.L. Dickert, and G.B. Witman. 1999. The DHC1b (DHC2) isoform of cytoplasmic dynein is required for flagellar assembly. *J. Cell Biol.* 144:473–481.

Perkins, L.A., E.M. Hedgecock, J.N. Thomson, and J.G. Culotti. 1986. Mutant sensory cilia in the nematode *Caenorhabditis elegans*. *Dev. Biol.* 117:456–487.

Pierce, D.W., and R.D. Vale. 1998. Assaying processive movement of kinesin by fluorescence microscopy. *Methods Enzymol.* 298:154–171.

Romberg, L., D.W. Pierce, and R.D. Vale. 1998. Role of the kinesin neck region in processive microtubule-based motility. *J. Cell Biol.* 140:1407–1416.

Rosenbaum, J.L., and G.B. Witman. 2002. Intraflagellar transport. *Nat. Rev. Mol. Cell Biol.* 3:813–825.

Scholey, J.M. 2003. Intraflagellar transport. *Annu. Rev. Cell Dev. Biol.* 19:423–443.

Setou, M., T. Nakagawa, D.H. Seog, and N. Hirokawa. 2000. Kinesin superfamily motor protein KIF17 and mLin-10 in NMDA receptor-containing vesicle transport. *Science*. 288:1796–1802.

Signor, D., K.P. Wedaman, J.T. Orozco, N.D. Dwyer, C.I. Bargmann, L.S. Rose, and J.M. Scholey. 1999a. Role of a class DHC1b dynein in retrograde transport of IFT motors and IFT raft particles along cilia, but not dendrites, in chemosensory neurons of living *Caenorhabditis elegans*. *J. Cell Biol.* 147:519–530.

Signor, D., K.P. Wedaman, L.S. Rose, and J.M. Scholey. 1999b. Two heteromeric kinesin complexes in chemosensory neurons and sensory cilia of *Caenorhabditis elegans*. *Mol. Biol. Cell.* 10:345–360.

Snow, J.J., G. Ou, A.L. Gunnarson, M.R. Walker, H.M. Zhou, I. Brust-Mascher, and J.M. Scholey. 2004. Two anterograde intraflagellar transport motors cooperate to build sensory cilia on *C. elegans* neurons. *Nat. Cell Biol.* 6:1109–1113.

Svoboda, K., and S.M. Block. 1994. Force and velocity measured for single kinesin molecules. *Cell*. 77:773–784.

Svoboda, K., C.F. Schmidt, B.J. Schnapp, and S.M. Block. 1993. Direct observation of kinesin stepping by optical trapping interferometry. *Nature*. 365:721–727.

Svoboda, K., P.P. Mitra, and S.M. Block. 1994. Fluctuation analysis of motor protein movement and single enzyme kinetics. *Proc. Natl. Acad. Sci. USA*. 91:11782–11786.

Thorn, K.S., J.A. Ubersax, and R.D. Vale. 2000. Engineering the processive run length of the kinesin motor. *J. Cell Biol.* 151:1093–1100.

Tomishige, M., D.R. Klopfenstein, and R.D. Vale. 2002. Conversion of Unc104/KIF1A kinesin into a processive motor after dimerization. *Science*. 297:2263–2267.

Vale, R.D. 2003. The molecular motor toolbox for intracellular transport. *Cell*. 112:467–480.

Wedaman, K.P., D.W. Meyer, D.J. Rashid, D.G. Cole, and J.M. Scholey. 1996. Sequence and submolecular localization of the 115-kD accessory subunit of the heterotrimeric kinesin-II (KRP85/95) complex. *J. Cell Biol.* 132:371–380.

Woehlke, G., A.K. Ruby, C.L. Hart, B. Ly, N. Hom-Booher, and R.D. Vale. 1997. Microtubule interaction site of the kinesin motor. *Cell*. 90:207–216.

Yamazaki, H., T. Nakata, Y. Okada, and N. Hirokawa. 1995. KIF3A/B: a heterodimeric kinesin superfamily protein that works as a microtubule plus end-directed motor for membrane organelle transport. *J. Cell Biol.* 130:1387–1399.

Yildiz, A., J.N. Forkey, S.A. McKinney, T. Ha, Y.E. Goldman, and P.R. Selvin. 2003. Myosin V walks hand-over-hand: single fluorophore imaging with 1.5-nm localization. *Science*. 300:2061–2065.

Zhang, Y., and W.O. Hancock. 2004. The two motor domains of KIF3A/B coordinate for processive motility and move at different speeds. *Biophys. J.* 87:1795–1804.